Available online at www.sciencedirect.com

SciVerse ScienceDirect

Ceramics International 38 (2012) 4961–4966

CERAMICS INTERNATIONAL

www.elsevier.com/locate/ceramint

Densification of SiO_2–cBN composites by using Ni nanoparticle and SiO_2 nanolayer coated cBN powder

Jianfeng Zhang, Rong Tu *, Takashi Goto

Institute for Materials Research, Tohoku University, Sendai 980-8577, Japan

Received 19 January 2012; received in revised form 28 February 2012; accepted 28 February 2012
Available online 7 March 2012

Abstract

Cubic boron nitride (cBN) powder was coated with Ni nanoparticle and SiO_2 nanolayer (abbreviated as cBN/Ni and cBN/SiO_2, respectively) by rotary chemical vapor deposition (RCVD), and compacted with SiO_2 powder by spark plasma sintering at 1473–1973 K for 0.6 ks. The effects of Ni and SiO_2 coatings on the densification, phase transformation of cBN and hardness of SiO_2–cBN composites were compared. The phase transformation of cBN to hBN was identified at 1973 K in SiO_2–cBN/SiO_2 composites, 300 K higher than that in SiO_2–cBN/Ni composites, indicating that SiO_2 retarded the transformation of cBN. The relative density of SiO_2–cBN/SiO_2 with 50 vol% cBN sintered at 1873 K was 99% with a hardness of 14.5 GPa.

Keywords: Ni nanoparticle; SiO_2 nanolayer; Cubic boron nitride (cBN); Rotary CVD (RCVD); Spark plasma sintering

1. Introduction

Silicon dioxide (SiO_2) is a most common oxide material with excellent insulation performance, high chemical stability, low thermal expansion coefficient and low thermal conductivity [1,2]. Thus, it can be used as structural materials, refractory material in crucibles, electronic circuit boards and semiconductors. However, due to its low hardness and toughness, the application of SiO_2 as a structural material has been limited. On the other hand, cubic boron nitride (cBN) has been widely used in cutting tools or as a reinforcing component to enhance the hardness and wear resistance due to its second highest hardness next to diamond, high thermal conductivity and less reactivity with iron than diamond [3–6]. Therefore, SiO_2–cBN composite can be a candidate structural material. However, the phase transformation of cBN to hexagonal BN (hBN) degrades the mechanical properties of cBN-based composite and the additives or second phase would significantly affect the phase transformation of cBN [7–10].

The phase transformation temperature of cBN to hBN (T_{cBN}) of Al_2O_3–Ni–cBN [9], WC–Co–cBN [10,11] and Al_2O_3–cBN [12] composites could be 1573–1673 K, lower than that of monolithic cBN [7] and TiN–cBN composite [13] (1873 K). In SiAlON–cBN [7,14,15], mullite–cBN [16] and SiO_2–cBN [17] composites, the T_{cBN} was at 1923–1973 K, 50–100 K higher than that of cBN. Therefore, the element of Si would retard the transformation of cBN. We have prepared SiO_2–cBN composites by spark plasma sintering at 1473–1973 K using commercial SiO_2 and cBN powders. The SiO_2–20 vol% cBN composite sintered at 1673 K showed the highest mechanical properties (hardness: 12.5 GPa; fracture toughness: 1.5 MPa $m^{1/2}$), and the cBN content could not be increased more than 30 vol% mainly due to the self-contact among cBN particles [17]. In order to prevent the self-contact of cBN particles, SiO_2 coating directly on cBN powder may be promising, and Ni nanoparticle precipitated on cBN powder could accelerate the densification of cBN-based composite at low temperature [9].

In the present study, cBN powder was first coated by Ni nanoparticle or SiO_2 nanolayer by rotary chemical vapor deposition (RCVD) [18] and compacted with SiO_2 by spark plasma sintering. The effects of Ni nanoparticle and SiO_2 nanolayer on the microstructures and mechanical properties of the SiO_2–cBN composite were investigated.

* Corresponding author.
E-mail address: turong@imr.tohoku.ac.jp (R. Tu).

0272-8842/$36.00
doi:10.1016/j.ceramint.2012.02.090

2. Experimental details

The ideal sintering aids are to fully coat the cBN powder with a minimum amount in order to prevent the performance degradation of cBN. Based on our preliminary work, the optimized conditions for coating uniform Ni or SiO_2 on cBN were selected as follows. Ni or SiO_2 was prepared on cBN powders (2–4 μm in diameter) by RCVD using nickelocene ($NiCp_2$) or tetraethyl orthosilicate (TEOS) at a supply rate of 0.8×10^{-6} kg s^{-1} and 11.1×10^{-9} m^3 s^{-1}. The deposition temperature was kept at 823 or 973 K for the coating of Ni or SiO_2, respectively. The CVD chamber was rotated at a rate of 45 rpm at 800 Pa for 1.8 ks. The Ni or SiO_2 coated cBN powders (abbreviated as cBN/Ni and cBN/SiO_2, respectively) were mixed with SiO_2 (0.5 μm in diameter) by ball milling. The mixed powders were compacted by spark plasma sintering (SPS-210LX, SPS Syntex Inc.) at 1473–1973 K and 100 MPa. The heating rate was 1.67 K s^{-1}, and the holding time was 0.6 ks. The temperature was measured by an optical pyrometer focusing on a hole (∅2 mm × 5 mm) in the graphite die.

The crystal phase was examined by X-ray diffraction (XRD; Geigerflex, Rigaku Corp.) with Cu Kα radiation. The Ni and Si contents were examined by an inductively coupled plasma-optical emission spectrometer (ICP-OES, IRIS Advantage Duo, Thermo Fisher Scientific, Waltham, USA). The microstructure was observed by transmission electron microscopy (TEM; JEOL: JEM-2000EX) and scanning electron microscopy (SEM, Hitachi: S-3100H). The density was determined by an Archimedes method, and the relative density was calculated using theoretical densities of SiO_2 (2.20 g/cm^3) [19], cBN (3.49 g/cm^3) [20] and Ni (8.91 g/cm^3) [21]. Vickers hardness (H_v) at room temperature was measured using a micro-hardness tester (HM-221, Mitutoyo) at a load of 9.8 N calculated from the following formula:

$$H_v = 1854 \times \frac{P}{d^2} \quad (1)$$

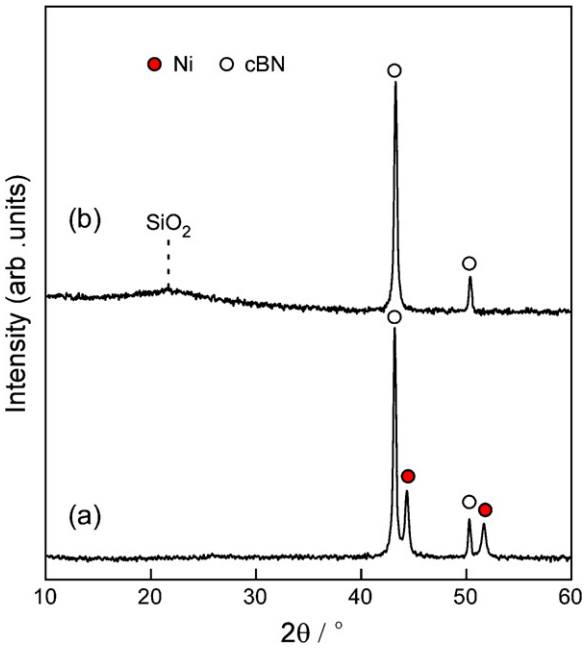

Fig. 1. XRD patterns of: (a) cBN/Ni and (b) cBN/SiO_2 powders.

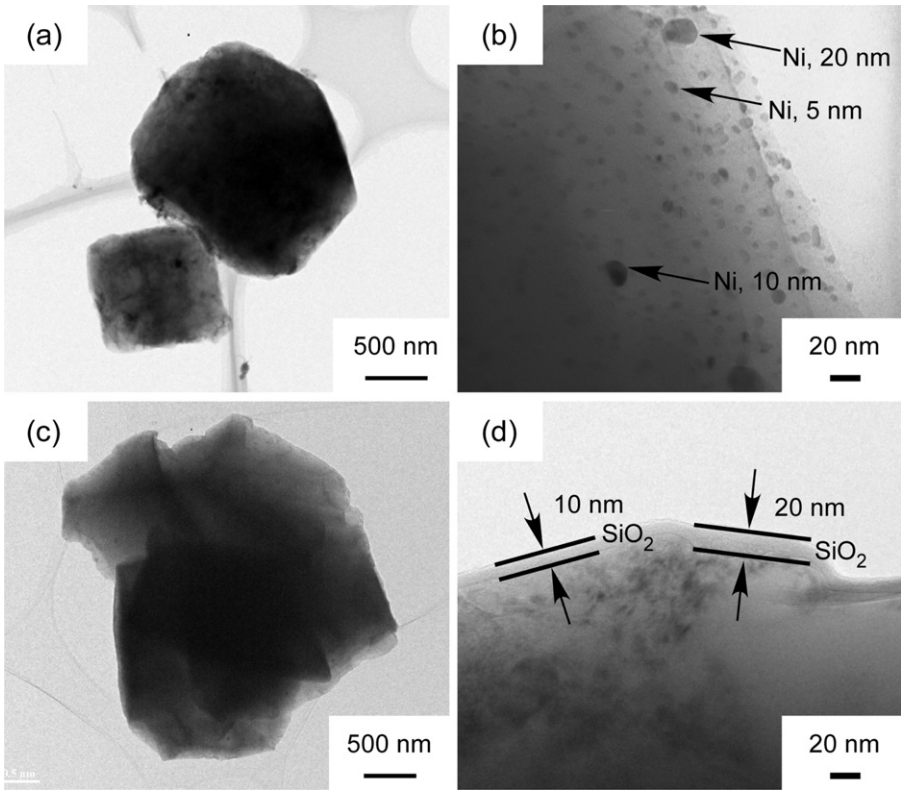

Fig. 2. TEM images of: (a and b) cBN/Ni and (c and d) cBN/SiO_2.

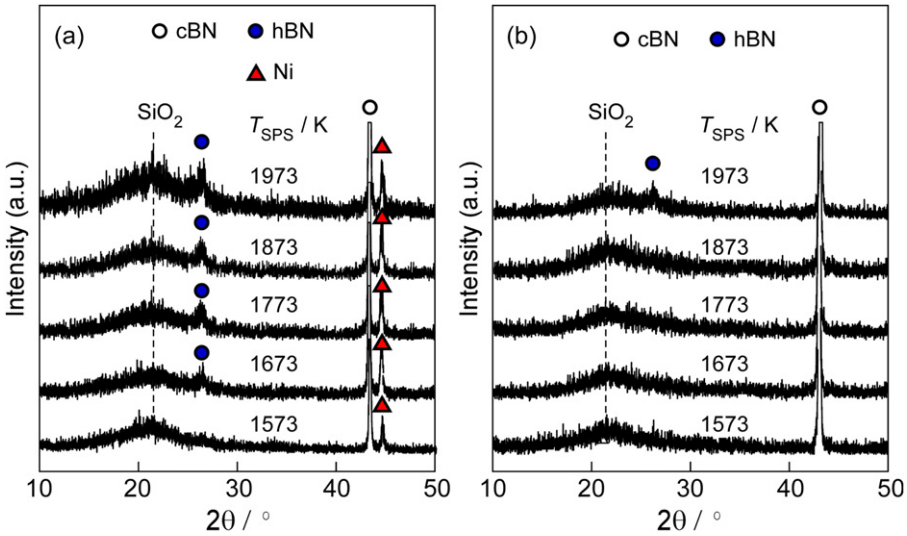

Fig. 3. XRD patterns of: (a) SiO_2–50 vol% cBN/Ni and (b) SiO_2–50 vol% cBN/SiO_2 composites sintered at 1573–1973 K.

where P (N) is the applied load and d (m) is the average value of the two diagonal lengths for Vickers indentation. The average value of 10 measurements at each specimen was used as the Vickers hardness.

3. Results and discussion

Fig. 1 shows the XRD patterns of cBN/Ni and cBN/SiO_2 powders. The peaks at $2\theta = 43.2^\circ$(1 1 1), 50.3°(2 0 0) and $2\theta = 21.6^\circ$(1 1 1) were indexed to Ni and SiO_2, respectively. A broad halo peak of SiO_2 indicated that SiO_2 phase was amorphous. Fig. 2 shows the TEM images of cBN/Ni and cBN/SiO_2 powders. The Ni nanoparticle (1.0 mass%, 5–20 nm in diameter) and SiO_2 nanolayer (1.9 mass%, 10–20 nm in thickness) were precipitated on cBN powders. The amorphous SiO_2 nanolayer has been reported to form by thermal decomposition of TEOS, i.e., by scission of the residual O–C bonds and reorientation of the Si–O bonds with remaining Si=O fragments [22]. The Si=O bonds represent the very beginning of the SiO_2 amorphous nanolayer formation. On the other hand, the thermal decomposition of $NiCp_2$ produced a thermodynamically unstable NiCp and then NiCp will further decomposed to Ni [23].

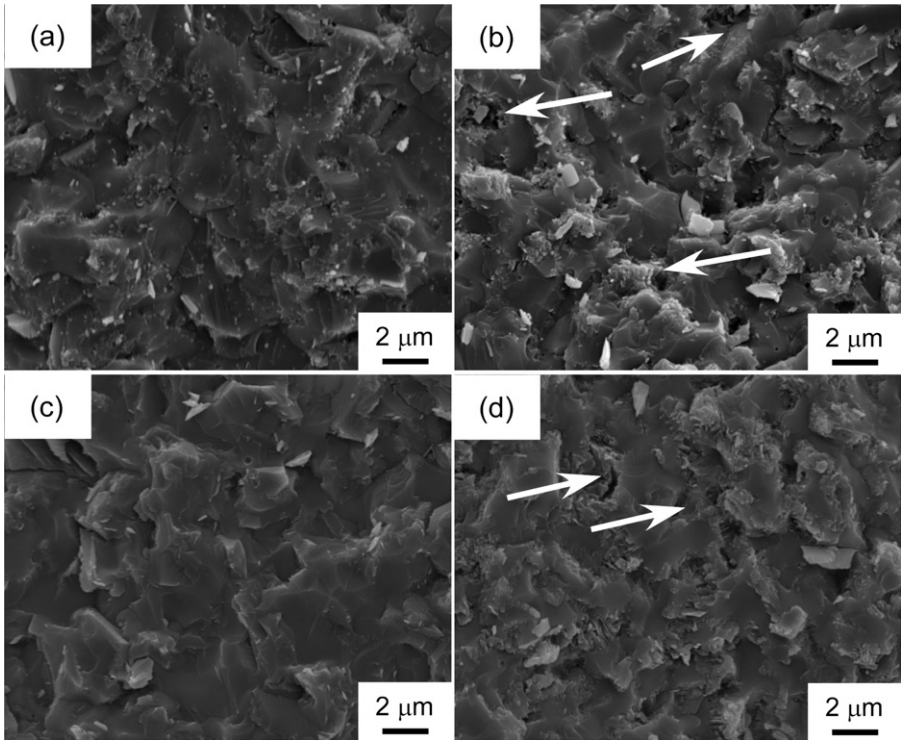

Fig. 4. Fracture surface images of SiO_2–50 vol% cBN/Ni composite sintered at (a) 1673 and (b) 1773 K, and SiO_2–50 vol% cBN/SiO_2 composite sintered at (c) 1873 and (d) 1973 K.

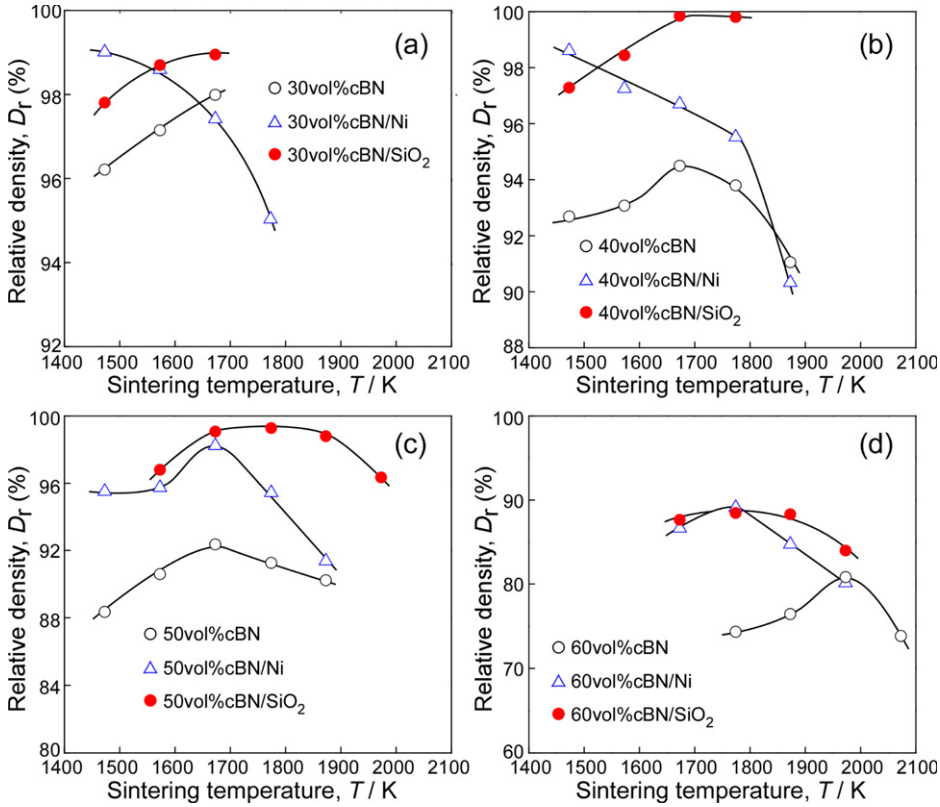

Fig. 5. Relative density of the SiO_2–cBN, SiO_2–cBN/Ni and SiO_2–cBN/SiO_2 composites sintered at 1473–2073 K.

Fig. 3 shows the XRD patterns of SiO_2–cBN/Ni and SiO_2–cBN/SiO_2 composites sintered at 1573–1973 K. The phase transformation of cBN to hBN was identified at T_{cBN} = 1673–1973 K in SiO_2–cBN/Ni composites, whereas the T_{cBN} was 1973 K in SiO_2–cBN/SiO_2 composites, about 300 K higher than that in SiO_2–cBN/Ni and 100 K higher than that in monolithic cBN [7]. This implies that the phase transformation of cBN to hBN was depressed by SiO_2 nanolayer while accelerated by Ni nanoparticles. Fig. 4 shows the SEM images of the fracture surface of SiO_2–50 vol% cBN/Ni composites sintered at 1673 and 1773 K and SiO_2–50 vol% cBN/SiO_2 composites sintered at 1873 and 1973 K. The BN grains were well adhered to and not with distinguished with at 1673 K in SiO_2–cBN/Ni composite and at 1873 K in SiO_2–cBN/SiO_2 composites, whereas a flake-like phase (white arrows) was identified in the SiO_2 matrix. The flake-like phase was a typical characteristic of the hBN phase transformed from cBN as observed in Al_2O_3–cBN [8], SiAlON–cBN [7] and mullite–cBN [16] composites.

Fig. 5 shows the relative density (D_r) of the SiO_2–cBN/Ni and SiO_2–cBN/SiO_2 composites sintered at 1473–2173 K compared with SiO_2–cBN composite without precipitation. The D_r of SiO_2–30 vol% cBN/Ni was 99% at 1473 K, higher than that of SiO_2–30 vol% cBN and SiO_2–30 vol% cBN/SiO_2. The D_r of SiO_2–30 vol% cBN and SiO_2–30 vol% cBN/SiO_2 increased with increasing temperature whereas the D_r of SiO_2–cBN/Ni decreased. This implies that Ni nanoparticle densified of SiO_2–cBN composite at low temperatures. The relative density of SiO_2–(40–50) vol% cBN/Ni showed the maximum value of 98% at 1673 K. The relative density of SiO_2–(40–50) vol% cBN/SiO_2 sintered at 1573–1873 K was close to 99%. The SiO_2 nanolayer precipitated on cBN was effective to

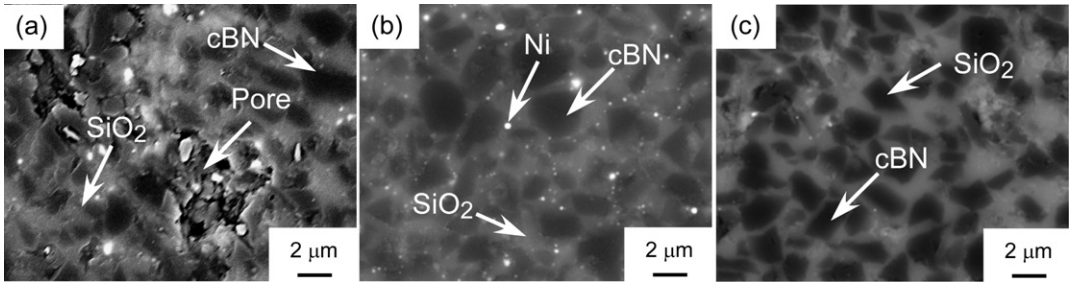

Fig. 6. Surface images of: (a) SiO_2–50 vol% cBN, (b) SiO_2–50 vol% cBN/Ni, and (c) SiO_2–50 vol% cBN/SiO_2 composites sintered at 1673 K.

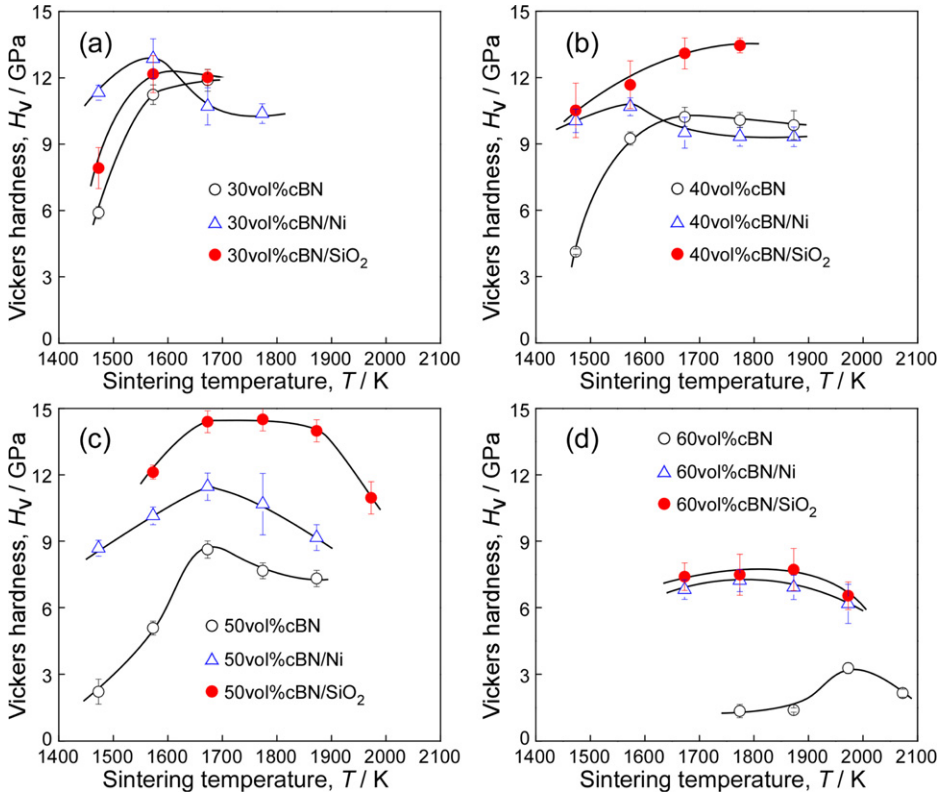

Fig. 7. Hardness of the SiO_2–cBN, SiO_2–cBN/Ni and SiO_2–cBN/SiO_2 composites sintered at 1473–2073 K.

increase the relative density of the SiO_2–cBN composites at high temperatures. The relative density of SiO_2–60 vol% cBN composites was lower than 90%.

Fig. 6 shows the microstructures of SiO_2–50 vol% cBN, SiO_2–50 vol% cBN/Ni and SiO_2–50 vol% cBN/SiO_2 composites sintered at 1673 K. Pores were identified in the SiO_2–50 vol% cBN whereas the SiO_2–50 vol% cBN/Ni and SiO_2–50 vol% cBN/SiO_2 composites were almost fully dense. Ni nanoparticles and SiO_2 nanolayer precipitated on cBN were effective to promote the densification of SiO_2–cBN composites.

Fig. 7 shows the hardness of the SiO_2–cBN, SiO_2–cBN/Ni and SiO_2–cBN/SiO_2 composites sintered at 1473–2173 K. The maximum hardness of SiO_2–30 vol% cBN, SiO_2–30 vol% cBN/Ni, SiO_2–30 vol% cBN/SiO_2 were 11.9, 12.9 and 12.2 GPa, respectively. Ni nanoparticle precipitated on cBN was effective to increase the hardness of SiO_2–cBN composites at low temperatures. With increasing temperature to 1673 K, the hardness of SiO_2–30 vol% cBN/Ni decreased to 10.7 and 10.4 GPa due to the phase transformation of cBN to hBN. Fig. 7(b) and (c) show that the SiO_2 nanolayer increased the maximum hardness of SiO_2–40 vol% cBN and 50 vol% cBN to 13.5 GPa and 14.5 GPa, respectively.

4. Conclusions

Ni nanoparticle and SiO_2 nanolayer were precipitated on cBN powder by RCVD. The cBN/Ni and cBN/SiO_2 powder were compacted with SiO_2 by SPS. Phase transformation of cBN to hBN occurred at 1973 K in SiO_2–cBN/SiO_2, 300 K higher than that in SiO_2–cBN/Ni composites. The relative density of SiO_2–(40–50) vol% cBN/SiO_2 sintered at 1573–1873 K was 99%. The highest hardness of SiO_2–cBN/SiO_2 was 14.5 GPa at 50 vol% cBN/SiO_2.

Acknowledgements

This research was financially supported by the Rare Metal Substitute Materials Development Project, New Energy and Industry Technology Development Organization (NEDO), by the Global COE Program (International Center of Education and Research) "Materials Integration, Tohoku University", and by the International Collaboration Center, ICC-IMR, Tohoku University.

References

[1] R.K. Brow, M.L. Schmitt, A survey of energy and environmental applications of glass, J. Eur. Ceram. Soc. 29 (2009) 1193–1201.
[2] T. Kokubo, Bioactive glass ceramics: properties and applications, Biomaterials 12 (1991) 155–163.
[3] R.H. Wentorf, R.C. DeVries, F.P. Bundy, Sintered superhard materials, Science 208 (1980) 873–880.
[4] K. Brookes, Making hardmetal even harder with dispersed cBN, Met. Powder Rep. 62 (2007) 14–17.
[5] N. Narutaki, Y. Yamane, Tool wear and cutting temperature of cBN tools in machining of hardened steels, Ann. ICRP 28 (1979) 23–28.
[6] H.O. Pierson, Handbook of Refractory Carbides and Nitrides, William Andrew Publishing/Noyes, 1996.
[7] M. Hotta, T. Goto, Densification and phase transformation of β-SiAlON–cubic boron nitride composites prepared by spark plasma sintering, J. Am. Ceram. Soc. 92 (2009) 1684–1690.

[8] M. Hotta, T. Goto, Densification and microstructure of Al_2O_3–cBN composites prepared by spark plasma sintering, J. Ceram. Soc. Jpn. 116 (2008) 744–748.
[9] J. Zhang, R. Tu, T. Goto, Spark plasma sintering of Al_2O_3–cBN composites facilitated by Ni nanoparticle precipitation on cBN powder by rotary chemical vapor deposition, J. Eur. Ceram. Soc. 31 (2011) 2083–2087.
[10] V. Martínez, J. Echeberria, Hot isostatic pressing of cubic boron nitride–tungsten carbide/cobalt (cBN–WC/Co) composites: effect of cBN particle size and some processing parameters on their microstructure and properties, J. Am. Ceram. Soc. 90 (2007) 415–424.
[11] B. Yaman, H. Mandal, Spark plasma sintering of Co–WC cubic boron nitride composites, Mater. Lett. 63 (2009) 1041–1043.
[12] M. Hotta, T. Goto, Effects of cubic BN addition and phase transformation on hardness of Al_2O_3–cubic BN composites, Ceram. Int. 37 (2011) 1453–1457.
[13] M. Hotta, T. Goto, Spark plasma sintering of TiN–cubic BN composites, J. Ceram. Soc. Jpn. 118 (2010) 137–140.
[14] M. Hotta, T. Goto, Spark plasma sintering of βSiAlON–cBN composite, Mater. Sci. Forum 561–565 (2007) 599–602.
[15] M. Hotta, T. Goto, Effect of time on microstructure and hardness of βSiAlON–cubic boron nitride composites during spark plasma sintering, Ceram. Int. 37 (2011) 521–524.
[16] M. Hotta, T. Goto, Densification, phase transformation and hardness of mullite–cubic BN composites prepared by spark plasma sintering, J. Ceram. Soc. Jpn. 118 (2010) 157–160.
[17] J. Zhang, R. Tu, T. Goto, Densification, microstructure and mechanical properties of SiO_2–cBN composites by spark plasma sintering, Ceram. Int. 38 (2012) 351–356.
[18] J. Zhang, R. Tu, T. Goto, Preparation of Ni-precipitated hBN powder by rotary chemical vapor deposition and its consolidation by spark plasma sintering, J. Alloys Compd. 502 (2010) 371–375.
[19] JCPDS, International Centre for Diffraction Data, No. 27-0605.
[20] JCPDS, International Centre for Diffraction Data, No. 25-1033.
[21] JPCDS, International Centre for Diffraction Data, No. 65-0380.
[22] J. Spitzmüller, J. Braun, H. Rauscher, R.J. Behm, Thermal decomposition of tetraethoxysilane (TEOS) on Si (1 1 1) − (7 × 7), Appl. Phys. A 66 (1998) s1021–s1024.
[23] L. Brissoneau, R. Sahnoun, C. Mijoule, C. Vahlas, Investigation of nickelocene decomposition during chemical vapor deposition of nickel, J. Electrochem. Soc. 147 (2000) 1443–1448.